ACS APPLIED MATERIALS & INTERFACES

www.acsami.org

Research Article

Rapid, Sensitive, Label-Free Electrical Detection of SARS-CoV-2 in Nasal Swab Samples

Hyun-June Jang, Wen Zhuang, Xiaoyu Sui, Byunghoon Ryu, Xiaodan Huang, Min Chen, Xiaolei Cai, Haihui Pu, Kathleen Beavis, Jun Huang, and Junhong Chen*

Cite This: *ACS Appl. Mater. Interfaces* 2023, 15, 15195−15202

Read Online

ACCESS | Metrics & More | Article Recommendations | Supporting Information

ABSTRACT: Rapid diagnosis of coronavirus disease 2019 (COVID-19) is key for the long-term control of severe acute respiratory syndrome coronavirus 2 (SARS-CoV-2) amid renewed threats of mutated SARS-CoV-2 around the world. Here, we report on an electrical label-free detection of SARS-CoV-2 in nasopharyngeal swab samples directly collected from outpatients or in saliva-relevant conditions by using a remote floating-gate field-effect transistor (RFGFET) with a 2-dimensional reduced graphene oxide (rGO) sensing membrane. RFGFET sensors demonstrate rapid detection (<5 min), a 90.6% accuracy from 8 nasal swab samples measured by 4 different devices for each sample, and a coefficient of variation (CV) < 6%. Also, RFGFET sensors display a limit of detection (LOD) of pseudo-SARS-CoV-2 that is 10 000-fold lower than enzyme-linked immunosorbent assays, with a comparable LOD to that of reverse transcription-polymerase chain reaction (RT-PCR) for patient samples. To achieve this, comprehensive systematic studies were performed regarding interactions between SARS-CoV-2 and spike proteins, neutralizing antibodies, and angiotensin-converting enzyme 2, as either a biomarker (detection target) or a sensing probe (receptor) functionalized on the rGO sensing membrane. Taken together, this work may have an immense effect on positioning FET bioelectronics for rapid SARS-CoV-2 diagnostics.

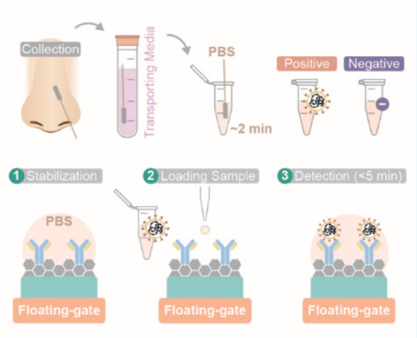

KEYWORDS: *rapid COVID-19 tests, FET COVID sensors, SARS-CoV-2, reduced graphene oxide, nasal swab testing, saliva testing*

■ INTRODUCTION

Coronavirus disease 2019 (COVID-19), causing more than 700 million infections and over six million deaths as of February 2023 (https://covid19.who.int/), has neutralized traditional containment measures such as the isolation of symptomatic individuals via epidemiological surveillance due to a large share of symptom-free but infectious carriers of severe acute respiratory syndrome coronavirus 2 (SARS-CoV-2);[1,2] indeed, SARS-CoV-2 affects all walks of our life. The emergence of new variants in recent years poses renewed threats to COVID-19 containment and to vaccine and drug efficacy.[3,4] The post-COVID-19 era questions now how consecutive exposures to different variants of virus shape population immunity, thereby modulating following epidemic cycles and disease burden.[5] The agenda definitely accompanies essential needs of accurate but rapid diagnosis of COVID-19 over conventional diagnostic tests which fall into two main categories: molecular tests such as reverse transcription-polymerase chain reaction (RT-PCR) and immunoassays.[6,7]

RT-PCR, considered as the gold standard for SARS-CoV-2 diagnosis, directly detects RNAs of SARS-CoV-2 in nasopharyngeal and oropharyngeal swabs at central lab facilities.[8,9] Testing results can be delivered in 5 h to 2 days,[10] which still needs to be shortened. Reverse transcription loop-mediated isothermal amplification (RT-LAMP), however, facilitates at-home tests of RT-PCR as it does not require complex heating and cooling cycles for RNA amplification so that a reader device can be hand-held and simpler.[11] A small cartridge of RT-LAMP that integrates all lab processes matches the central lab, therefore, results in a high accuracy (>90%) measurement in about 20 min.[12] The cost per test, however, is too high for regular-basis tests to track COVID-19; World Health Organization (WHO) target product profiles for COVID-19 test kits suggest < \$20 per test.[13] Also, molecular tests are limited to identify individuals previously infected by SARS-CoV-2 with some possibility in a false negative result if respiratory specimens are contaminated, not properly collected or if an individual is tested too early after exposure to the virus or too late in their infection.[14]

Immunoassays such as enzyme-linked immunosorbent assay (ELISA) and lateral flow immunoassays (LFIAs) have gained significant attention because they are cheaper and easier to implement at the point of care (POC) or at-home tests as well

Received: January 9, 2023
Accepted: March 7, 2023
Published: March 20, 2023

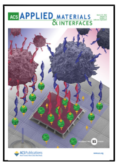

Table 1. Summary of Sensing Parameters of SARS-CoV-2 Detection Platforms

	Accuracy	Time	Cost	Throughput	Demand	Reference
RT-PCR	>90%	A few hours	Low	High	Clinical lab	9
RT-LAMP	>90%	<20 min	High	Low	At-home test, POC	12
LFIAs	56.2%	<5 min	Low	Low	At-home test	18
Our work	90.6%	<5 min	Low	Low	At-home test, POC	N/A

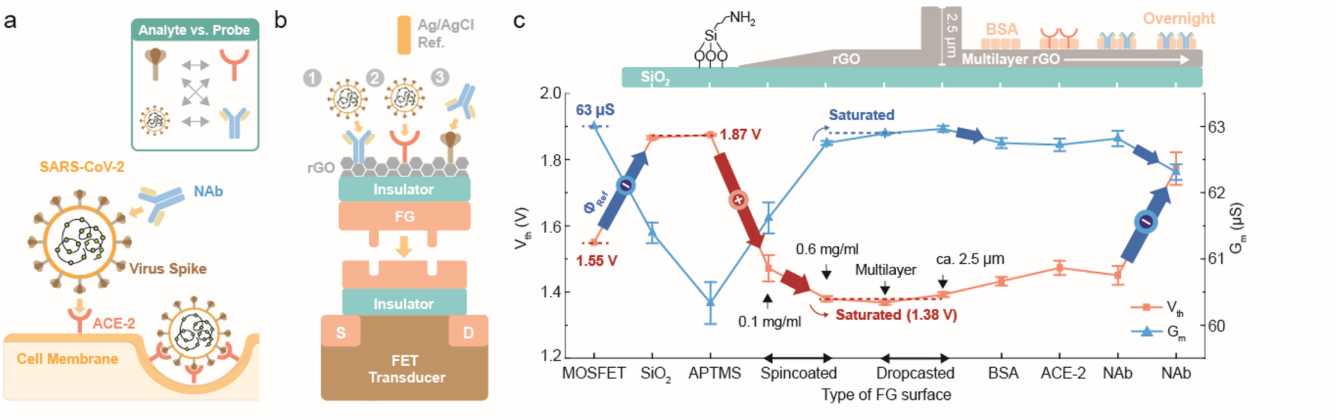

Figure 1. Schematic images of (a) infection process of SARS-CoV-2 mediated by the interaction between the viral SP and ACE-2 on the cell membrane; NAbs that are responsible for defending cells from pathogens are made by B-cells in the bone marrow. (b) Schematic images of label-free detection of SARS-CoV-2 using the RFGFET with either NAb or ACE-2 probes on rGO sensing layers of the RFG; a SP probe on rGO was also used for detection of NAbs. (c) V_{th} and G_m levels of the RFGFET changed by different surface conditions on the RFG; all RFGFETs were measured in the 1× PBS buffer solution using the same MOFEST and Ag/AgCl reference electrode.

as the ability to detect both antibodies and viral antigens.[15−17] Antibody tests identify a past infection and vaccination by detecting neutralizing antibodies (NAbs) developed in response to an infection in the blood. However, it takes a long turnaround period to receive results as blood collected from either a vein or a finger prick is transferred to medical facilities. Antigen tests with a POC or at-home test setting rapidly detect spike proteins (SPs) of the SARS-CoV-2 virus collected from the nasopharynx, anterior nares, and saliva; however, a Cochrane systemic review of 22 antigen test studies found that accuracy, which measures how often a test correctly gives a positive result when a person has the disease, varied considerably from 0% to 94% with the average accuracy being 56.2%.[18] This is not enough at all for diagnostic purposes of COVID-19. Indeed, there is a strong demand of a rapid diagnostic tool that is low-cost, accurate, and easy to use at home, as shown in Table 1.

From the early period of the pandemic, a few impressive field-effect transistor (FET) sensors have introduced rapid and direct detection of SARS-CoV-2 as a game changer.[19−21] Two-dimensional (2D) materials such as graphene, reduced graphene oxide (rGO), and MoS_2 with a high surface-to-volume ratio are proven to be highly sensitive to binding interactions between SARS-CoV-2 and receptors functionalized on 2D materials.[19,20] The FET sensors not only eliminate the multiple laboratory steps to amplify RNA or to immobilize the specialized reagents or enzymatic labels but also offer low-cost production, rapid detection (<1 min testing time), and a higher sensitivity than any of the conventional immunoassays and RT-PCR.[22−27]

Such a high sensitivity from 2D FET sensors particularly creates a great value proposition for the saliva testing approach at POC, which is simpler, faster, and easier to collect samples than nasopharyngeal swabs and blood. Despite the outstanding performance of FET sensors, none of the COVID-19 FET sensors has been approved by the Food and Drug Administration (FDA) for emergency use so far. An underlying challenge mainly stems from a lack of device reliability, reproducibility, and adequate control over the manufacturing quality of 2D semiconductors for large-scale production.[28−30] The success of COVID-19 FET sensors depends on how reliable and stable sensors can be achieved for mass production. In our previous work, a remote floating-gate (RFG) structure proposed for a 2D rGO layer eliminates non-reliable behaviors of solution interfacial properties remaining in a high surface-to-volume ratio at the sensing zone.[29] To be specific, the RFG structure enables to avoid any undesirable effects from interface traps, defects, and redox reactions of 2D rGO sensing membrane, which produces a high yield of signal and reproducibility.

In this paper, we report on a direct label-free detection of SARS-CoV-2 in nasopharyngeal swab samples collected from outpatients by utilizing rGO RFGFETs. We observed a 90.6% accuracy of SARS-CoV-2 from 8 deidentified nasopharyngeal swab sample tests, which were measured by 4 different devices for each sample; half of 8 nasal swab samples had been tested as positive and negative by RT-PCR while two nasal swap samples tested as positive had extremely low viral loads with cycle threshold (CT) values of 34 and 37 that are close to the detection limit of RT-PCR (CT = 40). The coefficient of variation (CV) of our raw electrical signals was <6%; CV value is a statistical measure of the relative dispersion of data points in a data series around the mean. For potential applications of our sensing platform for saliva tests, we also demonstrated the detection of pseudo-SARS-CoV-2 diluted in artificial saliva. NAb probes functionalized on rGO for detection of pseudo-SARS-CoV-2 revealed a sensing response at 3.2 mV/dec, a limit of detection (LOD) of 5×10^{-2} TU/ml in artificial saliva,

https://doi.org/10.1021/acsami.3c00331
ACS Appl. Mater. Interfaces 2023, 15, 15195−15202

which is $10^3\times$ lower than that of ELISA performed in PBS buffer condition (50 TU/ml), and a CV < 5%. A sensing response of 5.3 mV/dec was shown for spike protein (SP) of SARS-CoV-2 in artificial saliva, with a LOD of ~pg/mL and a CV < 3%.

We also characterized interactions between SP, NAb, angiotensin-converting enzyme 2 (ACE-2), and SARS-CoV-2 in phosphate-buffered saline (PBS) solutions, as either a probe or a biomarker. NAb probes for SP showed a sensing response of 6.5 mV/dec and a LOD of ~pg/mL while ACE-2 probes showed a slightly reduced sensing response (4.7 mV/dec) with a LOD of ~pg/mL but a lower CV < 2% than the NAb probe. SP probes to capture NAbs presented a sensing response of 6.7 mV/dec with an order of magnitude lower LOD (subpicogram per ml) than the reciprocal arrangement. This performance was accomplished through highly reliable RFGFETs with 2D rGO layers, enabling insignificant intrinsic device-to-device variations (CV < 2%) regardless of thicknesses of rGO and contact areas of media on the rGO.

RESULTS AND DISCUSSION

RFGFET Detection Platform. SARS-CoV-2 gains entry into target cells via an initial binding interaction between the SP and the ACE-2 receptor on the host cell surface, followed by viral fusion and entry (Figure 1a).[31] NAbs are responsible for defending cells from pathogens such as SARS-CoV-2, which are produced naturally by the body as part of its immune response against infections or vaccinations. NAb and ACE-2, functionalized on multilayer rGO sensing layers on the RFG (Figure 1b), are ideal probes for label-free detection of SARS-CoV-2 in patient specimens. Likewise, SP is used as a probe for the detection of NAb to identify a past infection and the efficacy of a vaccine.

Major technical hurdles of 2D FET biosensors include a non-reliable charge transport of the 2D FET transducer caused by non-uniform distributions of 2D materials, defects, and interface traps over the substrates; the solution environment on top of 2D FETs adds up additional uncontrollable variables such as redox reactions and ion diffusion.[29] The other reliability issue is also provoked by non-specific binding occurring in the FET sensing system, which is especially critical for 2D FETs as non-specific binding signals are also amplified by a high surface-to-volume ratio of 2D materials. Taken together, a low yield of sensitivity and thus a poor reliability of 2D FET biosensors are true pain points for market products of COVID-19 diagnostics.

An origin of instability such as drifts and hysteresis in 2D FET sensors (Figure S1) stems from a current flow over 2D materials, which is a source of energy to activate undesirable factors in 2D materials such as defects and interface traps. The RFG structure proposed for multilayer rGO (Figure 1b), however, blocks current flows over rGO during operations (Figure S2) due to a high input impedance on the gate section and enables a high surface-to-volume ratio of 2D rGO layers (<4 nm, Figure S3) as being isolated by a SiO_2 insulator and confined on a solution interface only; i.e., rGO layers on the RFG are capacitively coupled to the gate of metal-oxide-semiconductor FET (MOSFET). For our RFGFET design, the gate input impedance of the MOSFET was at least 100 times higher than that of the RFG structure (Figure S4). This enables the threshold voltage (V_{th}) of the RFGFET to be an independent variable from the impedance of RFG modules such as the thickness of SiO_2 and rGO (Figure 1c) and contact areas of a media solution on the RFG (Figure S5) so that the V_{th} of the RFGFET reflects intrinsic electrochemical properties of the FG surface. This RFG configuration is a key for high reproducibility in characterization of intrinsic electrochemical properties of rGO shown in Figure 1c.

To be specific, the MOSFET without connecting to the RFG has V_{th} (1.55 V) and transconductance (G_m) (63 μS), which is highly stable over repeating measurements (Figure S6). It is noted that 63 μS is a maximum G_m that could be shown for our RFGFET setup if the solution interface on the RFG is highly conductive. The V_{th} of the MOSFET increases up to 1.87 V when non-conductive SiO_2 and (3-aminopropyl)-trimethoxysilane (APTMS)/SiO_2 surfaces are added on the RFG (Figure 1c); G_m of the MOSFET (63 μS) decreases down to 61.3 and 60.3 μS for SiO_2 and APTMS/SiO_2, respectively. The increase in V_{th} is mostly attributed to the addition of the electrode potential of the Ag/AgCl reference electrode (ϕ_{ref}, 0.316 V). As rGO nanosheets were deposited on non-conductive APTMS/SiO_2 substrates by spin-coating the 0.1 mg/mL GO solution, V_{th} dramatically decreased (1.47 V) while increasing G_m (61.6 μS) (Figure 1c); the reduction in V_{th} is due to supplies of positive charges on the RFG solution interface from rGO networks including a large number of hole carriers. Saturation in V_{th} and G_m occurs near 1.38 V and 62.9 μS, respectively, by increasing concentrations of a spin-coating solution from 0.1 to 0.6 mg/mL or introducing full coverage of multilayers GO over the APTMS/SiO_2 surface using a heat-assisted drop-casting method.[29]

Interestingly, the V_{th} of highly thick rGO layers (ca. 2.5 μm, Figure S7) made by drop-casting even showed a similar level of V_{th} (1.39 V) to those of multilayer rGO (1.38 V). This is because the MOSFET recognized them as the same rGO interfaces regardless of the thickness of rGO on the RFG due to the input impedance of the MOSFET 100× higher than the RFG. This led to a promising way to characterize intrinsic interfacial potentials of the RFG surface independent of phyiscal properties of rGO on the RFG. Likewise, contact areas of a testing solution on rGO interfaces had no effects on V_{th} levels of the RFGFET, while V_{th} was only influenced by surface potential changes due to varying pH (Figure S5). As a result, the V_{th} of RFGFETs of pristine multilayer rGO was highly uniform and reproducible with a low CV < 2% which was calculated from raw V_{th} values of 8 devices (Figure S8).

The V_{th} of rGO RFGFET further responded to biomolecules functionalized on the surface of the pristine rGO (Figure 1c). Bovine serum albumin (BSA) on multilayer rGO as a blocking layer (no probe) slightly increased V_{th} (1.43 V) and decreased G_m (62.7 μS) relative to those of pristine multilayer rGO (V_{th}: 1.38 V, G_m: 62.9 μS). This indicates that binding non-conductive BSA on rGO screened positively charged, conductive rGO surfaces. The RFGFETs produced similar levels of V_{th} and G_m to those of BSA-blocked rGO (no probe) after adding probes of ACE-2 and NAb on rGO with BSA blocking. Overnight incubation of BSA, however, significantly increased V_{th} close to those of SiO_2 and APTMS/SiO_2 with a distinguishable reduction in G_m. This implies that immobilized BSA protein layers mostly shielded the charged rGO surfaces.

Detection of SARS-CoV-2 in PBS. Before clinical sample testing, we performed a systematic analysis on interactions between SP, NAb, and ACE-2 in a controlled buffer condition such as 0.05× PBS (pH 7.4). Addition of SPs on NAb probes induced additional positive charges[32] on the rGO surface (Figure 2a); ΔV_{th} was calculated as a difference in V_{th} at a

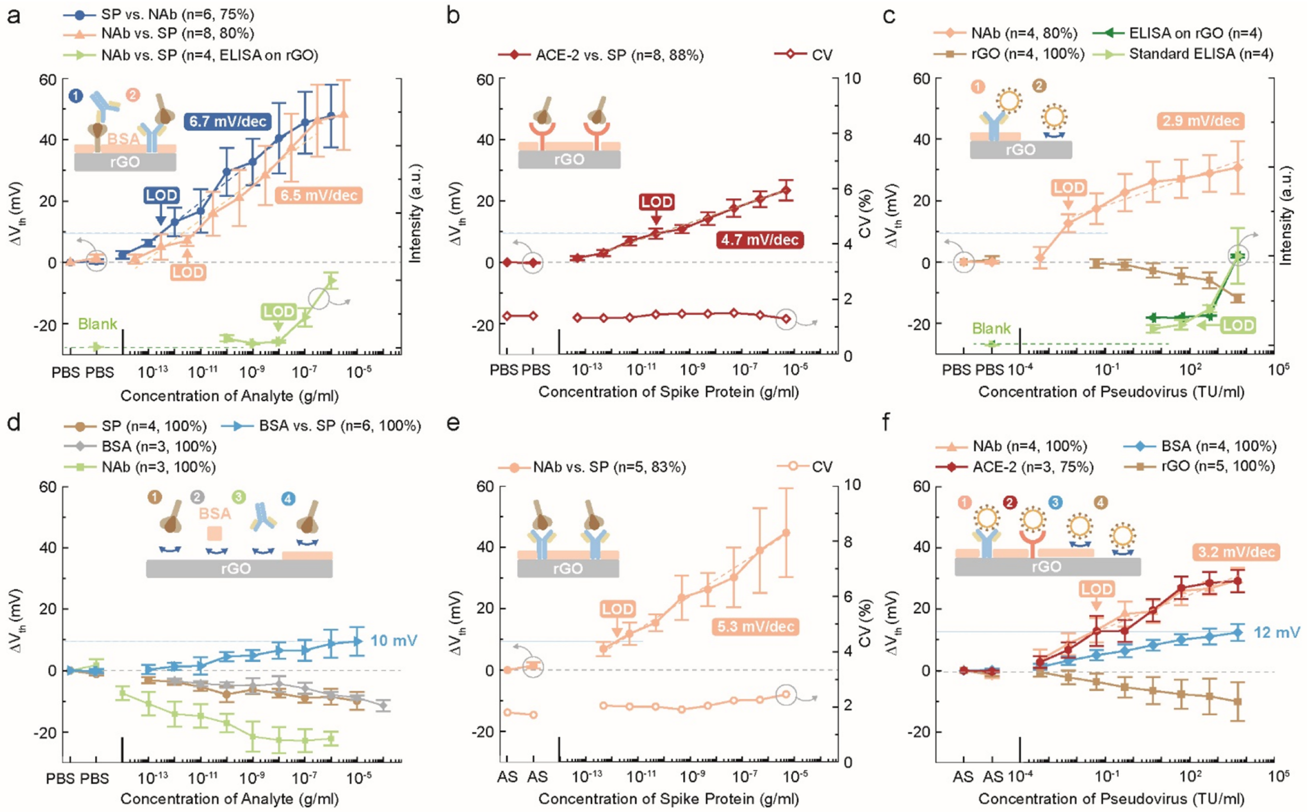

Figure 2. (a) ΔV_{th} of rGO with NAb or SP probes vs concentrations of SP or NAb in PBS, respectively. ELISA signals (NAb probes on rGO substrates vs SP) were compared. (b) ΔV_{th} and CV value of rGO with ACE-2 probes vs concentrations of SP in PBS. (c) ΔV_{th} of rGO with NAb probe or pristine rGO vs concentrations of pseudo-SARS-CoV-2 in PBS; ELISA measurements performed on a standard well plate and rGO substrates were compared. (d) ΔV_{th} of pristine rGO vs concentrations of SP, BSA, and NAb, respectively, and ΔV_{th} of BSA-blocked rGO vs SP. (e) ΔV_{th} of rGO with NAb probes vs concentrations of SP in artificial saliva mixture. (f) ΔV_{th} of rGO with NAb or ACE-2 probes vs concentrations of pseudo-SARS-CoV-2 in artificial saliva mixture and ΔV_{th} of BSA-blocked rGO or pristine rGO vs concentrations of pseudo-SARS-CoV-2 in artificial saliva mixture.

concentration of each analyte and a baseline V_{th} measured in the pure PBS prior to injections of analyte on the RFG. A sensing response of SP was measured to be 6.5 mV/dec in a range from 34 fg/mL to 340 ng/mL (R^2 of 0.97) over 6 samples (75% yield out of total 8) with the LOD at ∼a few pg/mL; we defined the LOD at the concentration of SP showing a clear signal in ΔV_{th} which was distinguishable from the maximum fluctuation in controls (ca. 10 mV), which will be discussed later in Figure 2d. CV of raw V_{th} levels for each concentration was less than 8% (Figure S9). ELISA performed on NAb-functionalized rGO substrates processed identically to the RFGFET showed 3 orders of magnitude higher LOD (∼a few ng/mL). SP probes reciprocally used for detection of NAb displayed a sensing response of 6.7 mV/dec in a range from 100 fg/mL to 100 ng/mL over 8 samples (80% yield out of total 10) with an order of magnitude lower LOD (subpg/mL) than the reciprocal arrangement (Figure 2a). Possibly, there is a smaller size of SP (26.54 kDa) than NAb (150k kDa) as probes mitigated Debye length issues or gave rise to higher probe densities on the rGO surface, which resulted in a lower LOD and a higher sensing response. On the other hand, ACE-2 probes presented a slightly reduced sensing response of 4.7 mV/dec (R^2 of 0.985) over 8 samples (88% yield out of total 9), compared to NAb probes, but with a wider dynamic range from 50 fg/mL to 5 μg/mL and higher uniformity in V_{th} signals (CV < 2%) (Figure 2b). This is possibly because ACE-2 has better orientations and uniformity at the rGO surface. Nonetheless, the LOD is at ca. 10 pg/mL due to its lower sensitivity and non-specific signals (Figure 2d), which could be further improved once background noise signals were suppressed. In order to increase the signal-to-noise ratio, NAb probes were routinely used for the following sections.

Using the NAb probes on the rGO surface, pseudo-SARS-CoV-2 was detected in 20 μL of PBS (Figure 2c). The sensitivity over background noises (ca. 10 mV) is measured to be 2.9 mV/dec (R^2 of 0.914) in a range from 5×10^{-3} to 5×10^3 TU/ml over 4 samples (80% yield out of total 5) with the LOD of 5×10^{-3} TU/ml. We compared ELISA results in Figure 2c using the same NAb probe for both standard well plate and rGO substrates. The LOD of ELISA performed on a standard well plate and rGO substrates (0.5 by 0.5 cm) was obtained at 50 and 500 TU/ml from 20 and 10 ul pseudo-SARS-CoV-2 dispersion, respectively. Such low LOD values from both RFGFETs (5×10^{-3} TU/ml) and ELISA (50 TU/ml) are possibly affected by detection of fragments of spike proteins in dispersion or inactive viral particles remaining in dispersion that cannot transduce cells. Nonetheless, our RFGFET showed a maximum of 10^4× lower LOD of pseudo SARS-CoV-2 in PBS for the same setup than ELISA, which agrees well with the results in Figure 2a.

Pristine rGO layers (no probe and blocking layer) showed a negative shifting trend in ΔV_{th} with increasing concentrations

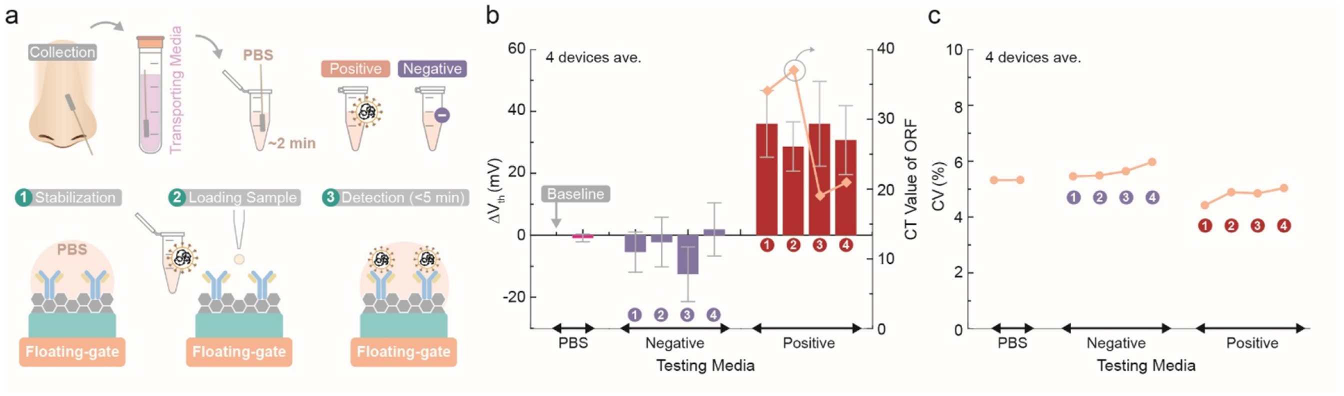

Figure 3. (a) Schematic images of a protocol for COVID-19 tests using the RFGFET. (b) ΔV_{th} distributions and CT values of rGO with NAb probes vs samples that have previously been tested as positive or negative. (c) CV calculated from raw V_{th} data of Figure 3b.

of pseudo-SARS-CoV-2 on pristine rGO layers. This is attributed to a strong non-specific binding between rGO and pseudo-SARS-CoV-2 due to hydrophobic interactions, which will be discussed further in Figure 2d.

A similar negative shifting trend in ΔV_{th} was shown over pristine rGO layers in contact with diverse types of proteins such as SP, BSA, and NAb (Figure 2d). This reaction typically accompanied reductions in G_m (Figure S10a). This RFGFET characterization suggested that there was a formation of a non-conductive interface on rGO by non-specific protein binding on rGO surfaces via hydrophobic bonding. It is noted that a specific binding signal in Figure 2a had no changes in G_m (Figure S10b), indicating the specific signal was triggered by changes in surface potentials resulting from interactions between receptor and analyte. This result highlights the importance of a blocking layer for FET sensors. However, BSA-blocked rGO layers (no probes but BSA incubation on top of the 1-pyrenebutanoic acid succinimidyl ester (PBASE) linker on rGO surface) also had non-specific binding signals but with a slight positive shifting trend in ΔV_{th} (Figure 2d), without G_m loss (Figure S10b). It is possibly attributed to the active PBASE linker on rGO to functionalize probes even after binding probes and BSA on rGO. We defined a maximum positive shift in ΔV_{th} (ca. 10 mV) in Figure 2d as the maximum background noise level of the RFGFET to determine the LOD. The LOD of our RFGFET can be lowered if this noise level is reduced by using different types of blocking layers such as polyethylene glycol (PEG).[33,34]

Detection of SARS-CoV-2 in Artificial Saliva. For the potential saliva testing approach of our sensing platform, we demonstrated detection of SP (Figure 2e) or pseudo-SARS-CoV-2 (Figure 2f) in artificial saliva mixed with PBS. PBS in this mixture plays a role of fixing the pH of testing media at pH 7.4 (Figure S11). Controlling the pH of testing media solution is especially important for FET sensing platforms as the pH of patients' saliva varying in a range from 6.2 to 7.6 could affect surface charges of proteins on sensing surfaces. A reduced SP sensing response (5.3 mV/dec in a range from 500 fg/mL to 5 μg/mL with an R^2 of 0.98) was shown from artificial saliva (Figure 2e), compared to those in PBS (6.5 mV/dec, Figure 2a), possibly due to a reduced Debye length by highly concentrated ions in artificial saliva. The LOD in this condition is at a few pg/mL and CV is <3%.

Pseudo-SARS-CoV-2 tests in the same saliva mixture showed a sensitivity of 3.2 mV/dec (R^2 of 0.94) in a range from 5×10^{-4} to 5×10^{3} TU/ml over 4 samples (100% yield out of total 4) in Figure 2f; an insignificant difference in sensing behavior is shown for two different probes such as NAb and ACE-2. BSA-blocked rGO (no probes) showed positive shifting of V_{th} in response to increasing concentrations of pseudo-SARS-CoV-2 in artificial saliva at a maximum of 12 mV, which is the maximum level of background noise in this system. According to this criterion, the LOD was calculated at 5×10^{-2} TU/ml, which is 10 times higher than those in PBS (Figure 2c). The LOD in artificial saliva is still 10^3 × lower than that of ELISA performed in PBS (50 TU/mL). Pristine rGO showed negative shifting in ΔV_{th} due to non-specific binding between rGO and protein surfaces, as was the case in Figure 2d.

Detection of SARS-CoV-2 in Real Patient Nasopharyngeal Swab Samples. Finally, deidentified clinical samples collected from outpatients at a clinical testing facility were tested with the protocol in Figure 3a. We prepared 12 nasopharyngeal swab samples (Figure 3b, Figure S13) in total that had been received in a 10 mL commercial universal transport medium; half of them had been tested as positive and negative by RT-PCR, respectively. Each nasopharyngeal swab was immersed in 100 μL (Figure 3b) or 1 mL of 0.05× PBS (Figure S13) for 2 min to transfer virus particles into PBS with a controlled pH at 7.4. Before injecting testing samples on the devices, the rGO surface on the RFG was stabilized under the pure 0.05× PBS to set a baseline of the measurement system. After stabilization, another pure 0.05× PBS solution was added to the RFG surface to double check if the baseline is maintained. After washing the surface with 0.05× PBS, 20 μL of the testing samples prepared above were injected into the RFG with NAb-functionalized rGO. Each rGO device was measured 20 times within 5 min. ΔV_{th} was calculated at a difference between V_{th} of each sample and a baseline V_{th} measured in a pure PBS prior to injections of samples.

Figure 3b shows ΔV_{th} distributions of RFGFETs measured from 8 nasopharyngeal swab samples (half tested positive and negative, respectively) which were diluted in each 100 μL PBS. Each test sample was measured by 4 different rGO devices; distributions of raw data of ΔV_{th} are shown in Figure S12. The baseline fluctuated in a range from −3 to 3 mV over all devices. Samples tested as positive displayed positive ΔV_{th} levels in a range from 23 to 84 mV over all tests (Figure S12); this positive ΔV_{th} corresponded to signals of SP (Figure 2a, 2e) and pseudo-SARS-CoV-2 (Figure 2c) on NAb probes. Clear sensing signals were even obtained from samples that had low viral loads (CT values: 34 and 37, which are close to the

https://doi.org/10.1021/acsami.3c00331
ACS Appl. Mater. Interfaces 2023, 15, 15195−15202

detection limit of RT-PCR at CT 40). However, ΔV_{th} signals were not proportional to CT values yet due to possible randomized concentrations of SARS-CoV-2 by additional transportation of patient nasal swab samples to PBS as shown in Figure 3a.

In contrast, ΔV_{th} levels of samples tested as negative mostly displayed negative ΔV_{th} or partially small positive ΔV_{th} in a range from −41 to 24 mV (Figure S12); herein, the maximum positive ΔV_{th} (24 mV) out of 16 negative testing devices was defined as a maximum background noise level of this system. The accuracy of the RFGFET was estimated to be 90.6% over the total 32 testing devices, which was calculated as the rate of RFGFETs to show distinguishable SARS-CoV-2 signals from the maximum background noise levels (24 mV); 3 testing results out of 32 revealed ΔV_{th} near the noise level at 24 mV (Figure S12). Moreover, CV calculated from raw V_{th} values for each sample (not ΔV_{th}) is less than 6% (Figure 3c), implying that our sensing signals are highly reproducible even for clinical sample testing. Four more nasopharyngeal swab samples (half tested positive and negative, respectively) were diluted in 1 mL PBS solution instead of a 100 μL PBS in order to investigate influences of dilution ratio on electrical RFGFET signals (Figure S13a). A similar detection trend was shown for this condition but overall levels of ΔV_{th} are much lowered than those in Figure 3a. Accuracy of this case was measured to be 62.5% over the total 8 devices due to highly diluted conditions for nasopharyngeal swab samples.

CONCLUSION

The emergence of new variants of SARS-CoV-2 in recent years put more concern on a potential increase in virulence, transmissibility, hospitalizations, and reinfections, all of which largely put stress on healthcare resources and potentially lead to more deaths. Viruses endlessly mutate over time and rapid diagnosis of COVID-19 is key for the long-term control of SARS-CoV-2. Central lab tests are inappropriate for a rapid diagnostic purpose; current at-home tests are either not sensitive enough (LFIAs) or too expensive (RT-LAMP). We demonstrated a rapid (ca. 5 min testing time) and direct detection of SARS-CoV-2 from both nasopharyngeal swab samples directly collected from outpatients and saliva-relevant media by using an rGO-based RFGFET. Our testing results show 90.6% accuracy and high reproducibility in signals (CV < 6% calculated from raw V_{th} data) from clinical sample tests despite additional dilutions of nasal swab samples. This additional transportation process could be omitted if the nasal samples are directly collected in PBS buffer solution at pH7.4. Also, the RFGFET has a high device yield (>75%) for all detection work due to structural advantages of the RFG proposed for 2D rGO sensing layers. This overcomes chronic and main issues of FET sensors for market products such as non-uniform electrical characteristics, irreproducibility, low yield, and device instability. This platform may have an immense effect on positioning FET bioelectronics in a clinical setting for COVID-19 detection.

EXPERIMENTAL METHODS

RFG Module Fabrication. The cleaned 4-in silicon wafer with a 300 nm-thick SiO_2 was treated with an oxygen plasma for 5 min at 250 W under an O_2 flow rate of 10 sccm in order to introduce hydroxyl groups on SiO_2 surfaces. The wafer was fully immersed and incubated in a 5% APTMS (Sigma-Aldrich, 281778) solution dissolved in ethanol (Sigma-Aldrich, 459836) for 2 h. After washing the surface, the wafer was heated at 120 °C for 20 min. GO solutions of 0.24 mg/mL were prepared by dispersing GO (ACS Material, 7782-42-5) in deionized water aided by ultrasonication for 20 min. Sixteen ml of 0.24 mg/mL GO solution was drop-casted over the entire area of a 4-in wafer and then baked at 120 °C for 1 h to obtain multilayer GO on APTMS-treated SiO_2 surface. The GO/APTMS/SiO_2 wafers were sliced to 1 × 2 cm^2 for the RFG module. The postannealing of the RFG module was performed using a horizontal furnace for 5 min under an argon gas environment, with a temperature of 400 °C. The fabricated rGO RFG modules were fully immersed in a 10 mg/mL 1-pyrenebutyric acid *N*-hydroxysuccinimide ester (PBASE) (Santa Cruz Biotechnology, 114932-60-4) diluted in dimethylformamide (DMF) for 2 h. After washing the rGO surfaces by DMF, 250 μg/mL SARS-CoV-2 NAb (Sino Biological, 40592-MM57) was incubated on the rGO surface for at least 2 h. Sequentially, a 10 mg/mL BSA solution dissolved in 1× PBS was added for at least 2 h. The SARS-CoV-2 SP (Sino Biological, 40592-V08B) was diluted in 0.05 × PBS to concentrations of 34 fg/mL to 3.4 μg/mL for testing media. Also, SP was diluted in a mixture of solution between 0.05× PBS and artificial saliva (Fisher Scientific, NC1873811) with a ratio of 20:1 to concentrations of 500 fg/mL to 5 μg/mL for testing media. The initial pH of the artificial saliva was 6. Pseudo SARS-CoV-2 purchased from Integral Molecular was diluted in 0.05× PBS or artificial saliva mixture in a range from 5×10^{-4} to 5×10^{3} TU/ml. Twelve deidentified nasopharyngeal swab samples were received in a commercial universal transporting media from the University of Chicago Medicine. The clinical samples (nasopharyngeal swabs) used in this study (Figure 3) were collected from human subjects as part of registered protocols approved by the Institutional Review Board of UChicago Medicine. Six nasopharyngeal swab samples were previously tested as positive by RT-PCR. The remaining specimens were tested as negative. Each nasopharyngeal swab was immersed in either 100 μL or 1 mL of 0.05× PBS for 2 min as the testing media solution.

ELISA Protocol. The standard sandwich ELISA was performed in a new 48-well plate. For ELISA of the RFG, the antibody-conjugated rGO substrates sliced to 0.5 × 0.5 cm^2 were placed on a new 48-well plate. Each well plate and RFG sensing membrane was functionalized with 250 μg/mL NAb with a BSA blocking layer and was washed gently three times with 1× PBS including 0.05% Tween 20. To block non-specific binding and reduce the background of the well plate, a 500 μL of 1× assay diluent buffer was added per well and incubated at RT for 1 h with shaking at 300 rpm on a plate shaker. For the ELISA of SP (Sino Biological, 40592-V08B), a 500 μL SP solution prepared in 1× assay buffer with different concentrations was incubated on each well and rGO RFG, respectively, for 2 h under 300 rpm at room temperature for detection of SP. A SP solution of 20 and 10 μL was placed for each well and rGO RFG, respectively. For the ELISA of pseudo-SARS-CoV-2 (Biolegend), 500 μL of SP pseudo-SARS-CoV-2 prepared in 1× assay buffer with different concentrations was incubated on each well and rGO RFG, respectively, for 2 h under 300 rpm at room temperature for detection of pseudo-SARS-CoV-2. A pseudo-SARS-CoV-2 solution of 20 and 10 μL was placed for each well and rGO RFG, respectively. After gently washing each well and rGO RFG three times with 1× PBS including 0.05% Tween 20, 500 μL of anti-SARS-CoV-2 avidin-HRP (Biolegend) or 500 μL anti-SARS-CoV-2 spike-HRP (Abcam) diluted 1000 times in 1× assay buffer was incubated for 30 min with 300 rpm shaking under room temperature for detection of SP and pseudo-SARS-CoV-2, respectively, then gently washed five times using 1 × PBS including 0.05% Tween 20. The samples were soaked in the buffer for 30 s during each wash. Then, a 250 μL 3,3′,5,5′-tetramethylbenzidine substrate was further added into each well and incubated for 30 min under dark. Finally, a 100 μL stop reagent (2N H_2SO_4) was added, and the resulting solutions in each well were transferred to another new 96-well plate for measurement. The absorbance values were read at 450 and 570 nm using a microplate reader (Epoch, BioTek). Each point of ELISA data in Figure 2a and 3c is an average of at least four values.

Electrical Measurement System. A commercial MOSFET (CD4007UB) was used as a transducer to investigate the fabricated

RFG module. A 20 μL testing media solution prepared above was placed on the RFG module. An Ag/AgCl reference electrode contacted the testing media solution in order to apply the gate bias in a range from 0 to 5 V for all measurements. A n-type MOSFET was chosen as a transducer and used over all measurements consistently. All transfer curves were measured using a Keithley 4200A semiconductor analyzer with a drain voltage set at 50 mV, and the gate voltage remained in the double-sweep mode. Transfer curves of the RGFET were repeatedly measured for 20 cycles under each testing media solution. Each solution was removed by pipetting after each measurement. The V_{th} was calculated as the gate voltage corresponding to a drain current of 1 μA on each transfer curve. The G_m of each RGFET was calculated at its maximum value. Each ΔV_{th} point was obtained from the last point of ΔV_{th} in quasi-equilibrium for 20 measurements (5 min testing time) at each concentration.

■ ASSOCIATED CONTENT

Supporting Information

The Supporting Information is available free of charge at https://pubs.acs.org/doi/10.1021/acsami.3c00331.

> Stability, gate-current measurement, topographic image of 2D multilayers rGO, impedance of the RFG, contact area effect, electrical properties of the Si-FET transducer, SEM image of rGO films, CV values of raw data of V_{th} for each surface condition of RFG, CV values of raw data of V_{th} for each concentration of spike protein, G_m loss resulting from SP and BSA binding, pH variation up on dilutions of artrifical saliva, ΔV_{th} distributions of raw data from clinical sample tests, ΔV_{th} levels of rGO with NAb probes vs nasopharyngeal swab samples diluted in 1 mL of PBS (PDF)

■ AUTHOR INFORMATION

Corresponding Author

Junhong Chen − *Pritzker School of Molecular Engineering, University of Chicago, Chicago, Illinois 60637, United States; Chemical Sciences and Engineering Division, Physical Sciences and Engineering Directorate, Argonne National Laboratory, Lemont, Illinois 60439, United States;* orcid.org/0000-0002-2615-1347; Email: junhongchen@uchicago.edu

Authors

Hyun-June Jang − *Pritzker School of Molecular Engineering, University of Chicago, Chicago, Illinois 60637, United States; Chemical Sciences and Engineering Division, Physical Sciences and Engineering Directorate, Argonne National Laboratory, Lemont, Illinois 60439, United States*

Wen Zhuang − *Pritzker School of Molecular Engineering, University of Chicago, Chicago, Illinois 60637, United States; Chemical Sciences and Engineering Division, Physical Sciences and Engineering Directorate, Argonne National Laboratory, Lemont, Illinois 60439, United States*

Xiaoyu Sui − *Pritzker School of Molecular Engineering, University of Chicago, Chicago, Illinois 60637, United States; Chemical Sciences and Engineering Division, Physical Sciences and Engineering Directorate, Argonne National Laboratory, Lemont, Illinois 60439, United States*

Byunghoon Ryu − *Chemical Sciences and Engineering Division, Physical Sciences and Engineering Directorate, Argonne National Laboratory, Lemont, Illinois 60439, United States*

Xiaodan Huang − *Pritzker School of Molecular Engineering, University of Chicago, Chicago, Illinois 60637, United States*

Min Chen − *Pritzker School of Molecular Engineering, University of Chicago, Chicago, Illinois 60637, United States;* orcid.org/0000-0001-7856-8788

Xiaolei Cai − *Pritzker School of Molecular Engineering, University of Chicago, Chicago, Illinois 60637, United States*

Haihui Pu − *Pritzker School of Molecular Engineering, University of Chicago, Chicago, Illinois 60637, United States; Chemical Sciences and Engineering Division, Physical Sciences and Engineering Directorate, Argonne National Laboratory, Lemont, Illinois 60439, United States*

Kathleen Beavis − *Department of Pathology, University of Chicago, Chicago, Illinois 60637, United States*

Jun Huang − *Pritzker School of Molecular Engineering, University of Chicago, Chicago, Illinois 60637, United States;* orcid.org/0000-0003-0271-4384

Complete contact information is available at: https://pubs.acs.org/10.1021/acsami.3c00331

Notes

The authors declare no competing financial interest.

■ ACKNOWLEDGMENTS

This work was finally supported by a Walder Foundation grant and a University of Chicago Big Ideas Generator grant.

■ REFERENCES

(1) Zuin, M.; Gentili, V.; Cervellati, C.; Rizzo, R.; Zuliani, G. Viral Load Difference Between Symptomatic and Asymptomatic COVID-19 Patients: Systematic Review and Meta-Analysis. *Infect. Dis. Rep.* **2021**, *13*, 645−653.

(2) Subramanian, R.; He, Q. X.; Pascual, M. Quantifying Asymptomatic Infection and Transmission of COVID-19 in New York City Using Observed Cases, Serology, and Testing Capacity. *P. Natl. Acad. Sci. USA* **2021**, *118*, No. e2019716118.

(3) Burton, D. R.; Topol, E. J. Variant-proof Vaccines - Invest Now for the Next Pandemic. *Nature* **2021**, *590*, 386−388.

(4) Centers for Disease Control and Prevention. *SARS-CoV-2 Variant Classifications and Definitions* 2022, https://www.cdc.gov/coronavirus/2019-ncov/variants/variant-classifications.html.

(5) Sun, K.; Tempia, S.; Kleynhans, J.; von Gottberg, A.; McMorrow, M. L.; Wolter, N.; Bhiman, J. N.; Moyes, J.; du Plessis, M.; Carrim, M.; et al. SARS-CoV-2 Transmission, Persistence of Immunity, and Estimates of Omicron's Impact in South African Population Cohorts. *Sci. Transl. Med.* **2022**, *14*, eabo7081.

(6) Peck, K. R. Early Diagnosis and Rapid Isolation: Response to COVID-19 Outbreak in Korea. *Clin. Microbiol. Infec.* **2020**, *26*, 805−807.

(7) Singh, B.; Datta, B.; Ashish, A.; Dutta, G. A Comprehensive Review on Current COVID-19 Detection Methods: From Lab Care to Point of Care Diagnosis. *Sens. Int.* **2021**, *2*, 100119.

(8) Torretta, S.; Zuccotti, G.; Cristofaro, V.; Ettori, J.; Solimeno, L.; Battilocchi, L.; D'Onghia, A.; Bonsembiante, A.; Pignataro, L.; Marchisio, P.; et al. Diagnosis of SARS-CoV-2 by RT-PCR Using Different Sample Sources: Review of the Literature. *Ent- Ear Nose Throat J.* **2021**, *100*, 131s−138s.

(9) Arnaout, R.; Lee, R. A.; Lee, G. R.; Callahan, C.; Yen, C. F.; Smith, K. P.; Arora, R.; Kirby, J. E. SARS-CoV2 Testing: The Limit of Detection Matters. *bioRxiv* **2020**, DOI: 10.1101/2020.06.02.131144.

(10) Afzal, A. Molecular Diagnostic Technologies for COVID-19: Limitations and Challenges. *J. Adv. Res.* **2020**, *26*, 149−159.

(11) de Oliveira, K. G.; Estrela, P. F. N.; Mendes, G. D.; dos Santos, C. A.; Silveira-Lacerda, E. D.; Duarte, G. R. M. Rapid Molecular Diagnostics of COVID-19 by RT-LAMP in a Centrifugal Polystyrene-toner Based Microdevice with End-point Visual Detection. *Analyst* **2021**, *146*, 1178−1187.

(12) Giri, B.; Pandey, S.; Shrestha, R.; Pokharel, K.; Ligler, F. S.; Neupane, B. B. Review of Analytical Performance of COVID-19 Detection Methods. *Anal. Bioanal. Chem.* **2021**, *413*, 35−48.

(13) World Health Organization, COVID-19 Target Product Profiles for Priority Diagnostics to Support Response to the COVID-19 Pandemic v.1.0, 2020, https://www.who.int/publications/m/item/covid-19-target-product-profiles-for-priority-diagnostics-to-support-response-to-the-covid-19-pandemic-v.0.1.

(14) Sidiq, Z.; Hanif, M.; Dwivedi, K. K.; Chopra, K. K. Benefits and Limitations of Serological Assays in COVID-19 Infection. *Indian J. Tuberc.* **2020**, *67*, S163−S166.

(15) Jegerlehner, S.; Suter-Riniker, F.; Jent, P.; Bittel, P.; Nagler, M. Diagnostic Accuracy of SARS-CoV-2 Saliva Antigen Testing in a Real-Life Clinical Setting. *Int. J. Infect. Dis.* **2022**, *119*, 38−40.

(16) Mak, G. C. K.; Lau, S. S. Y.; Wong, K. K. Y.; Chow, N. L. S.; Lau, C. S.; Lam, E. T. K.; Chan, R. C. W.; Tsang, D. N. C. Analytical Sensitivity and Clinical Sensitivity of the Three Rapid Antigen Detection Kits for Detection of SARS-CoV-2 Virus. *J. Clin. Virol.* **2020**, *133*, 104684.

(17) Lake, D. F.; Roeder, A. J.; Kaleta, E.; Jasbi, P.; Pfeffer, K.; Koelbela, C.; Periasamy, S.; Kuzmina, N.; Bukreyev, A.; Grys, T. E.; et al. Development of a Rapid Point-of-Care Test that Measures Neutralizing Antibodies to SARS-CoV-2. *J. Clin. Virol.* **2021**, *145*, 105024.

(18) Dinnes, J.; Deeks, J. J.; Berhane, S.; Taylor, M.; Adriano, A.; Davenport, C.; Dittrich, S.; Emperador, D.; Takwoingi, Y.; Cunningham, J.; et al. Rapid, Point-of-Care Antigen and Molecular-based Tests for Diagnosis of SARS-CoV-2 Infection. *Cochrane Db. Syst. Rev.* **2022**, *8*, 1−131.

(19) Seo, G.; Lee, G.; Kim, M. J.; Baek, S. H.; Choi, M.; Ku, K. B.; Lee, C. S.; Jun, S.; Park, D.; Kim, H. G.; et al. Rapid Detection of COVID-19 Causative Virus (SARS-CoV-2) in Human Nasopharyngeal Swab Specimens Using Field-Effect Transistor-Based Biosensor. *ACS Nano* **2020**, *14*, 5135−5142.

(20) Li, J.; Wu, D.; Yu, Y.; Li, T.; Li, K.; Xiao, M. M.; Li, Y.; Zhang, Z. Y.; Zhang, G. J. Rapid and Unamplified Identification of COVID-19 with Morpholino-modified Graphene Field-Effect Transistor Nanosensor. *Biosens. Bioelectron.* **2021**, *183*, 113206.

(21) Guo, K. Y.; Wustoni, S.; Koklu, A.; Diaz-Galicia, E.; Moser, M.; Hama, A.; Alqahtani, A. A.; Ahmad, A. N.; Alhamlan, F. S.; Shuaib, M.; et al. Rapid Single-molecule Detection of COVID-19 and MERS Antigens via Nanobody-Functionalized Organic Electrochemical Transistors. *Nat. Biomed. Eng.* **2021**, *5*, 666−677.

(22) Kutovyi, Y.; Hlukhova, H.; Boichuk, N.; Menger, M.; Offenhausser, A.; Vitusevich, S. Amyloid-beta Peptide Detection via Aptamer-Functionalized Nanowire Sensors Exploiting Single-Trap Phenomena. *Biosens. Bioelectron.* **2020**, *154*, 112053.

(23) Alabsi, S. S.; Ahmed, A. Y.; Dennis, J. O.; Khir, M. H. M.; Algamili, A. S. A Review of Carbon Nanotubes Field Effect-Based Biosensors. *IEEE Access* **2020**, *8*, 69509−69521.

(24) Sarkar, D.; Liu, W.; Xie, X. J.; Anselmo, A. C.; Mitragotri, S.; Banerjee, K. MoS2 Field-Effect Transistor for Next-Generation Label-Free Biosensors. *ACS Nano* **2014**, *8*, 3992−4003.

(25) Kwong Hong Tsang, D.; Lieberthal, T. J.; Watts, C.; Dunlop, I. E.; Ramadan, S.; del Rio Hernandez, A. E.; Klein, N. Chemically Functionalised Graphene FET Biosensor for the Label-free Sensing of Exosomes. *Sci. Rep.* **2019**, *9*, 13946.

(26) Hwang, M. T.; Heiranian, M.; Kim, Y.; You, S.; Leem, J.; Taqieddin, A.; Faramarzi, V.; Jing, Y. H.; Park, I.; van der Zande, A. M.; et al. Ultrasensitive Detection of Nucleic Acids Using Deformed Graphene Channel Field Effect Biosensors. *Nat. Commun.* **2020**, *11*, 1543.

(27) Park, D.; Kim, J. H.; Kim, H. J.; Lee, D.; Lee, D. S.; Yoon, D. S.; Hwang, K. S. Multiplexed Femtomolar Detection of Alzheimer's Disease Biomarkers in Biofluids Using a Reduced Graphene Oxide Field-Effect Transistor. *Biosens. Bioelectron.* **2020**, *167*, 112505.

(28) Piccinini, E.; Fenoy, G. E.; Cantillo, A. L.; Allegretto, J. A.; Scotto, J.; Piccinini, J. M.; Marmisolle, W. A.; Azzaroni, O. Biofunctionalization of Graphene-Based FET Sensors through Heterobifunctional Nanoscaffolds: Technology Validation toward Rapid COVID-19 Diagnostics and Monitoring. *Adv. Mater. Interfaces* **2022**, *9*, 2102526.

(29) Jang, H. J.; Sui, X.; Zhuang, W.; Huang, X.; Chen, M.; Cai, X.; Wang, Y.; Ryu, B.; Pu, H.; Ankenbruck, N.; et al. Remote Floating-Gate Field-Effect Transistor with 2-Dimensional Reduced Graphene Oxide Sensing Layer for Reliable Detection of SARS-CoV-2 Spike Proteins. *ACS Appl. Mater. Interfaces* **2022**, *14*, 24187−24196.

(30) Jang, H. J.; Wagner, J.; Song, Y. J.; Lee, T.; Katz, H. E. Carboxylic Acid-Functionalized Conjugated Polymer Promoting Diminished Electronic Drift and Amplified Proton Sensitivity of Remote Gates Compared to Nonpolar Surfaces in Aqueous Media. *Adv. Electron. Mater.* **2020**, *6*, 1901073.

(31) Ke, Z. L.; Oton, J. Q.; Qu, K.; Cortese, M.; Zila, V.; McKeane, L.; Nakane, T.; Zivanov, J.; Neufeldt, C. J.; Cerikan, B.; et al. Structures and Distributions of SARS-CoV-2 Spike Proteins on Intact Virions. *Nature* **2020**, *588*, 498−502.

(32) Zamzami, M. A.; Rabbani, G.; Ahmad, A.; Basalah, A. A.; Al-Sabban, W. H.; Nate Ahn, S.; Choudhry, H. Carbon Nanotube Field-Effect Transistor (CNT-FET)-based Biosensor for Rapid Detection of SARS-CoV-2 (COVID-19) Surface Spike Protein S1. *Bioelectrochemistry* **2022**, *143*, 107982.

(33) Star, A.; Gabriel, J. C. P.; Bradley, K.; Gruner, G. Electronic Detection of Specific Protein Binding Using Nanotube FET devices. *Nano Lett.* **2003**, *3*, 459−463.

(34) Filipiak, M. S.; Rother, M.; Andoy, N. M.; Knudsen, A. C.; Grimm, S.; Bachran, C.; Swee, L. K.; Zaumseil, J.; Tarasov, A. Highly Sensitive, Selective and Label-free Protein Detection in Physiological Solutions Using Carbon Nanotube Transistors with Nanobody Receptors. *Sens. Actuat. B-Chem.* **2018**, *255*, 1507−1516.